Korean J. Chem. Eng., 36(4), 551-562 (2019)
DOI: 10.1007/s11814-019-0234-x

pISSN: 0256-1115
eISSN: 1975-7220

Activated carbon synthesized from biomass material using single-step KOH activation for adsorption of fluoride: Experimental and theoretical investigation

Parimal Chandra Bhomick, Aola Supong, Rituparna Karmaker, Mridushmita Baruah, Chubaakum Pongener, and Dipak Sinha†

Department of Chemistry, Nagaland University, Lumami 798627, India
(*Received 20 October 2018 • accepted 19 January 2019*)

Abstract–Single-step potassium hydroxide synthesized activated carbon was prepared from *Schima wallichii* biomass by optimizing process parameters at different carbonization temperature (500 °C, 600 °C, 700 °C and 800 °C) and biomass to KOH impregnation ratio (1 : 0, 1 : 1, 1 : 2 and 1 : 3). The optimum condition for obtaining the best activation carbon was found to be at 600 °C and 1 : 2 impregnation ratio with BET surface area, total pore volume, and pHzpc of 1,005.71 m^2g^{-1}, 0.491 cm^3g^{-1} and 6.11, respectively. SEM and XRD analysis revealed the ordering of the graphitic layer with more pores in the carbon matrix at optimized conditions. Batch adsorption experiments were run for fluoride adsorption and fitted, of which Langmuir isotherm model seems to be the best-fitted model with maximum adsorption capacity of 2.524 mgg^{-1}. Adsorption kinetics was elucidated best with the pseudo-second-order kinetic model. Theoretical calculations indicate that the adsorption of fluoride is favorable on edge site of both zig-zag and arm chair carbon models with chemisorption type of interaction. Fluoride uptake was found to be affected by the presence of co-ion in the order: $CO_3^{2-}>SO_4^{2-}>NO_3^->Cl^-$.

Keywords: *Schima wallichii* Biomass, Single-step Synthesis, Activated Carbon, Fluoride Adsorption, DFT

INTRODUCTION

Depletion of resources has already crossed the threshold point due to the increase in global population. Among various resources available, water is indispensable for the sustenance of life. However, with the rapid increase in industrialization and urbanization, access to safe and untainted water has become an emerging issue because of the sharp deterioration of the normal property of water with various contaminants: organic, radioactive, inorganic, and micropollutants etc. Out of various contaminants present in water, fluoride is one such element that pollutes the aquatic system both naturally and anthropogenically. Fluoride can be regarded as a "day and night" kind of an element, as it is both beneficial as well as hazardous based on its concentration. When taken in low quantity it proves propitious for the development of bones and teeth, but above 1.5 mg L^{-1} (permissible limit given by WHO), it becomes a health hazard. According to the World Health Organization, it is also considered as one of the drinking water contaminants in addition to arsenic and nitrate which cause large-scale health problems [1].

Long-term uptake of fluoride beyond the permissible limit can cause toxic symptoms, such as muscle fiber degeneration, thyroid disorder, Alzheimer's syndrome, dental fluorosis or even skeletal fluorosis [2,3]. It is estimated that around 70 million people globally suffer from fluorosis [4]. Fluoride concentration above the permissible level has been reported in many countries, especially in developed and developing countries, for example, U.S.A., China, Japan, Canada, Africa, and India [5]. In India, chronic amounts of fluoride around 12-18 mgL^{-1} have been reported with 17 states showing high fluoride content [2].

Thus, it is of great concern to control the fluoride concentration to a safe limit. Different remedies regarding removal of fluoride from water have been contrived over the years, as for instance nanofiltration (NF) [6], reverse osmosis (RO) [7], ion-exchange [8], electrodialysis [9], and adsorption [10]. Among these, adsorption accounts for an efficient method because of its cost-effectiveness, high efficiency, facile design, uncomplicated regeneration, and minimal chemical utility [11]. In this regard, therefore, activated carbon as an adsorbent has been comprehensively utilized for defluoridation studies owing to its excellent surface area, and surface reactivity. It is a versatile adsorbent that has been used extensively for various applications because of which its demand has been amplified over the years [12-15]. However, as it is synthesized from precursors like fossil-based raw materials or coal that are relatively expensive, making its extensive use somewhat limited [16]. This has ignited numerous researches to focus on obtaining alternative cost-effective materials in the production of activated carbon. Thus, agricultural and agro-based waste biomass has been gaining increased attention because of their cost-effectiveness, availability, eco-friendly characteristics and also due to renewability [13,15-23]. There have been numerous reports on synthesis of activated carbon from agricultural and animal residues with higher surface area, excellent porosity and surface functionalities [13,14,16,24-30].

Activated carbon preparation is done by physical or chemical activation. Physical activation requires carbonization of raw material in an inert atmosphere to remove non-carbon elements, fol-

†To whom correspondence should be addressed.
E-mail: dipaksinha@gmail.com

lowed by the activation with O_2, CO_2 or steam usually in the temperature range of 600-1,200 °C [31]. Chemical activation, on the other hand, is achieved by mixing carbon materials with chemical activating agents such as alkali metals (KOH, K_2CO_3, NaOH, Na_2CO_3), metal salts ($AlCl_3$, $FeCl_3$, $ZnCl_2$) and acids (H_3PO_4, HCl, H_2SO_4 HNO_3) followed by carbonization at 400-900 °C. Chemical activation is usually preferred as it gives rise to superior ordered structure activated carbon with higher surface area, pore volume and surface functionality [31]. Among the various chemical activating agents used, KOH is a widely used activating agent for generation of porous framework in the carbon with oxygen surface functionality [31]. These properties in carbon by KOH activation are mainly due to (a) etching of carbon structure brought about by the redox reaction of KOH with carbon materials, (b) reaction of in-situ generated H_2O and CO_2 with carbon, and (c) by intercalation of metallic potassium in the carbon lattices of the carbon matrix [31,32].

In a general preparation of activated carbon by KOH, two steps are involved: activation of raw precursor with KOH solution followed by carbonization at high temperature or vice versa [33-37]. However, replacing KOH solution with solid KOH reduces the number of activation steps to one step, making the preparation process more environmentally oriented. Thus, in the present work, a single step KOH activation step was followed for synthesis of the activated carbon by taking *Schima wallichii* biomass as the starting material.

Schima wallichii is an evergreen medium-to-large tree which attains a maximum height of 47 m and can grow in a wide range of climates, habitats, and soils [38]. The wood of the tree is used for construction purpose of medium to heavy type such as beams, flooring, interior fitting, and paneling. While its bark and tannin are used for dyeing and skin processing [38], but its seed cover is shredded without being used, and till date, no report on its usage is documented.

Thus, for the first time, this research utilized *Schima wallichii* biomass for activated carbon preparation using single step KOH activation because of the effectiveness of KOH in development of narrow pore size distribution and enhanced porosity. Therefore, keeping in view the advantage of single step synthesis and availability of the biomass material, we focused on the single-step KOH synthesis of activated carbon from *Schima wallichii* biomass by optimizing the activation processes (KOH impregnation ratio and activation temperature). Subsequently, application of the synthesized carbon for removal of fluoride from the aqueous medium was determined to evaluate the efficacy of the adsorbent developed by this method. Adsorption isotherm and kinetics studies were investigated. An insight into the fluoride adsorption onto activated carbon surface through theoretical study using DFT method was evaluated to comprehend the interaction mechanism. Effect of coexisting ions were also studied for understanding the efficacy of the prepared adsorbent.

MATERIALS AND METHODS

Schima wallichii seed cover was collected from the vicinity of Nagaland University, Lumami Campus (N26°13′29.3″/E094°28′34.6″, elevation 960.5 m), India and was used as the precursor for the synthesis of activated carbon. KOH, NaOH, HCl, NaCl, $NaNO_3$, Na_2CO_3, and Na_2SO_4 were purchased from HIMEDIA (India) while KNO_3 was obtained from Merck India. NaF purchased from Merck India was used to prepare Standard fluoride solution.

1. Preparation of *Schima wallichii* Activated Carbon (SWAC)

For the preparation of activated carbon, first, the collected *Schima wallichii* seed cover was granulated using mortar and pestle into smaller pieces and washed many times over with double distilled water to eliminate any impurities adhered to it. It was dried at 110 °C until all the moisture evaporated. The dried biomass sample was then triturated using a rotatory ball mill (Fritsch-Pulver Isette-7) into finer particles using Zirconium ball at 600 rpm for ten minutes. For the preparation of activated carbon, single-step activation was used in which the dried biomass sample was thoroughly mixed with different amount of solid KOH (1 : 1, 1 : 2 and 1 : 3), and was carbonized in an electrically heated muffle furnace at different temperatures (500-800 °C) under continuous nitrogen flow for 2 hrs at heating rate of 20 °C min^{-1}. The cooled carbonized black samples were then soaked in 0.5 M HCl solution for eight hours to completely remove any by-products formed during the activation process. The samples were then washed multiple times with hot water and finally with cold distilled water until the wash water final pH becomes neutral. The activated black carbon samples were then dried in a hot air oven for 24 hours at 110 °C and stored in a hermetically sealed container until further required. The activated samples were labeled as SWAC-Kxy, where K stands for KOH activation, x stands for impregnation ratio (1-3), and y is activation temperature (5=500 °C, 6=600 °C, 7=700 °C and 8=800 °C). Further for comparative study, one of the samples was carbonized without KOH impregnation (1 : 0). Yield percentage for the prepared carbons was calculated using the following equation:

$$\text{Yield of activated carbon (\%)} = \left(\frac{\text{mass of final carbon after activation process}}{\text{initial mass of the dry impregnated sample}}\right) \times 100$$

2. Characterization of Carbon Samples

To determine the physio-chemical nature, various analytical methods were used to characterize the samples. BET surface area and porosity were measured using BET surface area analyzer (Smart instrument, SS93/02) by measuring N_2 adsorption-desorption isotherm at liquid N_2 temperature (–195.79 °C) by degassing the samples at 300 °C for 60 minutes. Ash content was determined using ASTM method [39]. Elemental analysis was done using a CHN elemental Analyzer (Model: PE 2400 Series II, Make: Perkin Elmer). SEM analyses were performed with SEM Model: JSM-6360 (JEOL) to investigate the surface morphology and texture of carbon samples. The zero-point charge was measured by batch equilibrium method (Babic et al., 1999). Powdered XRD analysis involved using CuKα radiation at the scanning rate of 0.2 degree per minute by employing XRD (Model Rigaku-Ultima IV Japan). Surface functionality of the prepared carbon was analyzed using Fourier transform infrared (FT-IR) spectrometer (Model: Spectrum Two, Made: Perkin Elmer) (FT-IR spectra are given as supplementary data).

3. Batch Adsorption Experiments

Batch mode experiments were accomplished by taking 50 ml of

fluoride solution in a 250 ml Erlenmeyer flask stirred with a known amount of carbon in a rotary shaker at 150 rpm. After each experiment, the solution was filtered and the unadsorbed fluoride concentration was measured using a fluoride meter (Model Hanna Hi 98402 ISE Fluoride Meter). Mean values were taken as the final value, after running all the experiments in triplicates. The effect of adsorption conditions, like pH (2-12), adsorbent doses (0.1-0.6 g), contact time (2-180 mins) initial fluoride concentration (2 mgL^{-1}, 5 mgL^{-1} and 8 mgL^{-1}) was also studied. The removal efficiency (%) and the defluoridation capacity (mg g^{-1}) for SWAC were determined using Eq. (1) and (2), respectively:

$$\text{Removal efficiency}\,(\%)=\frac{C_0-C_e}{C_0}\times 100 \quad (1)$$

$$q_e=\frac{(C_0-C_e)V}{W} \quad (2)$$

where C_0 (mgL^{-1})=initial fluoride concentration; C_e (mgL^{-1})=fluoride concentration at equilibrium; W (g)=adsorbent dosage; V (L)= volume of solution used in batch experiment; q_e=adsorption capacity.

Adsorption isotherms studies are very essential as they give a clear idea about maximum adsorption capacity by establishing the extended mechanism between the adsorbate and the adsorbent of any system, thus providing economic viability in various commercial applications. Though numerous adsorption models are available, three well-known models, Langmuir, Freundlich and Temkin, are studied to understand the adsorption mechanism, adsorbate-adsorbent propinquity and the process favorability. Understanding the controlling mechanism of the adsorption process is of great import; thus to evaluate the adsorption kinetics of fluoride onto SWAC, pseudo-first and pseudo-second-order kinetic models were applied to probe the experimental data. The different models of adsorption isotherm and kinetics for this research are enumerated in Table 1.

Table 1. Equations for adsorption isotherm and Kinetic models

Models	Equation	References
Langmuir	$\frac{C_e}{q_e}=\frac{1}{Q_{max}K_L}+\frac{1}{Q_{max}}C_e$ $R_L=\frac{1}{1+K_LC_0}$	[40,41]
Freundlich	$\log q_e=\frac{1}{n_F}(\log C_e)+\log K_F$	[42]
Temkin	$q_e=B_T\ln A_T+B_T\ln C_e$	[43]
Pseudo-first-order kinetic	$\log(q_e-q_t)=\log q_e-\frac{k_1}{2.303}t$	[44]
Pseudo-second-order kinetic	$\frac{t}{q_t}=\frac{1}{k_2q_e^2}+\frac{t}{q_e}$	[45]

q_e=amount of adsorbate at equilibrium; K_L=Langmuir isotherm constant (L/mg); C_e=concentration of adsorbate at equilibrium (mgL^{-1}); C_0=initial adsorbate concentration (mgL^{-1}); q_{max}=maximum adsorption capacity; R_L=separation factor; n_F=Freundlich adsorption intensity; K_F=Freundlich isotherm constant; A_T and B_T=Temkin constant; q_t=adsorption capacity at time t (min); k_1= pseudo-first-order rate constant; k_2=pseudo-second-order rate constant

4. Theoretical Investigation for Fluoride Adsorption

Theoretical calculations were performed with Gaussian 09W program package to understand the adsorption of fluoride onto activated carbon using DFT method [46]. The geometry optimizations along with frequency calculations and energy calculations used the B3LYP method at basis set 6-31 g level of theory in a dielectric medium of ε=80 (corresponding to water). The polarizable continuum model (PCM) in G09 was used to estimate the influence of the solvent medium on the electronic structure of the solute and thereby to calculate the interaction energy between the solute and the dielectric medium. All of the models were produced using Gauss View 05 and were optimized in their electronic ground state. To generate an effectual site, carbon atoms on the cluster models were unsaturated on the upper side and the rest of the outer carbon atoms were terminated using hydrogen atoms [47].

The adsorption energy (E_{ad}) of Fluoride on carbon surface is calculated using the equation

$$E_{ad}=E_{adsobate-adsorbent}-(E_{adorbate}+E_{adsorbent})$$

where, $E_{adsobate-adsorbent}$ is the total energy of the fluoride/AC system in an equilibrium state; $E_{adsorbate}$ is the total energy of the adsorbate fluoride molecule; $E_{adsorbent}$ is the total energy of the AC system. Negative value of E_{ad} at the higher end accounts for a stronger adsorption. Usually, adsorption energy less that −30 kJ/mol indicates physisorption type of interaction and adsorption energy greater than −50 kJ belongs to chemisorption [48].

RESULTS AND DISCUSSION

1. Optimization of the Activation Condition

Optimization of activation condition plays a pivotal role in obtaining an adsorbent with superior property. Activation parameters such as impregnation ratio and activation temperature are considered as important factors for chemical activation method, as these parameters significantly modify the properties of the synthesized carbon. Impregnation of KOH leads to release of tars from the cross-linked skeleton because of reaction between the biomass and activating reagent. This leads to development of pores which ultimately modify the surface area and pore volume. While, activation temperature plays a role in production of microporous and mesoporous framework which affects the adsorption properties of an adsorbent. In the current work, an effort was made to understand the effect of impregnation ratio (biomass/KOH impregnation ratio of 1 : 1, 1 : 2 and 1 : 3) and activation temperature (500 °C, 600 °C, 700 °C and 800 °C) on the synthesized carbon properties since these different activation parameters had a significant effect on the surface area, yield, and porosity on the prepared carbon. The following section discusses the impact of the activation conditions on carbon properties.

1-1. Effect of Activation Temperature

Effect of activation temperature at different impregnation ratio is given in Table 2. It has been observed that with increasing activation temperature, the surface area of the carbon increases initially and then decreases with further increase in activation tem-

Table 2. Effect of activation parameters on yield % and BET surface area

Sample ID	Impregnation ratio SWB/KOH	Activation temperature (°C)	Yield (%)	BET surface area (m^2g^{-1})
SWAC-K05	1 : 0	500	43.38	92.32
SWAC-K06	1 : 0	600	39.27	112.83
SWAC-K07	1 : 0	700	30.06	198.30
SWAC-K08	1 : 0	800	26.31	152.24
SWAC-K15	1 : 1	500	30.13	407.45
SWAC-K16	1 : 1	600	27.46	652
SWAC-K17	1 : 1	700	24.02	625.66
SWAC-K18	1 : 1	800	20.85	543.12
SWAC-K25	1 : 2	500	19.17	687.66
SWAC-K26	1 : 2	600	18.84	1005.71
SWAC-K27	1 : 2	700	15.49	999.1
SWAC-K28	1 : 2	800	11.33	714.17
SWAC-K35	1 : 3	500	18.35	597.26
SWAC-K36	1 : 3	600	14.91	882.13
SWAC-K37	1 : 3	700	12.55	756.83
SWAC-K38	1 : 3	800	8.55	694.01

perature. Similar trend almost constitutes for all the carbon impregnated with different ratio of KOH. This could be probably because of the diffusion of volatile material from the carbon matrix due to the carbon gasification by KOH leading to the formation of new pores. But at a higher temperature of 700 °C and above, BET surface area was found to decrease, which might be due to rearrangement of carbon structure by enlargement and wrecking of the already prevailing in carbon. It was also observed that yield percentage of all the samples reduces with activation temperature, which could be due to volatilization and decomposition of the biopolymer compounds such as hemicellulose, cellulose and lignin existing in the biomass. When biomass material is heated during carbonization, surface functional groups present decompose to produce various volatile by-product like CO, H_2O and CO_2 leading to the decrease in the yield percentage of the adsorbent [33,49,50]. While analyzing the present results, the optimum condition for activations seems to be 1 : 2 KOH impregnation ratio with activation temperature of 600 °C, as highest BET surface area was achieved under this condition. Similar optimized activation conditions like impregnation ratio of KOH/biomass of 1 : 2 at 600 °C condition were reported by Singh and co-workers for preparation of activated carbon using biomass of *Arundo donax* [32].

1-2. Effect of Impregnation Ratio

The effect of impregnation ratio of *SWB*/KOH was investigated at an activation temperature of 600 °C to understand the role of KOH in initiating a chain reaction during carbonization. The BET surface area of 112.83 m^2g^{-1} of the carbon without KOH impregnation was found to increase to 652 m^2g^{-1} to 1,005.71 m^2g^{-1}, respectively, with KOH impregnation ratio of 1 : 1 to 1 : 2. This increase could be due to porosity formation by KOH activation.

However, it was observed that this trend decreased at higher impregnation ratio of 1 : 3. This decrease might be due to the widening and opening of pores leading to shrinkage of the carbon matrix resulting from over-oxidation of carbon walls by CO_2 and CO gases released during KOH activation [26,27]. The decrease could also be due to the formation of more highly insoluble potassium residues with a higher amount of KOH at 1 : 3 ratio.

Similarly, pore volume of the samples were also seen to increase from 0.061 to 0.491 cm^3g^{-1} and thereafter decreased at impregnation ratio of 1 : 3, probably due to the existing pore widening in the carbon matrix. Similar findings on the impact of impregnation ratio on surface area and porosity have also been highlighted in the literature [32,33,49,51-53].

Table 3 also shows the basic elemental composition of activated carbon prepared using different KOH impregnation ratio at an optimized temperature of 600 °C. The carbon content was found to increase with KOH impregnation till the ratio became 1 : 2. Whereas, hydrogen content increased with KOH impregnation, reflecting that KOH is a suitable chemical agent that accelerates dehydrogenation. Similarly, the decrease in oxygen and nitrogen content upon KOH activation activated carbon was probably due to easy stripping of oxygen and nitrogen by potassium hydroxide.

From the above experiments, it was found that the maximum surface area could be achieved when activation was done at a temperature of 600 °C with 1 : 2 impregnation ratio. The carbons synthesized under this condition were further analyzed for elemental analysis and point of zero charge to estimate the carbon content and surface charge. The activated carbon produced by this method had higher carbon content (84.25%), making it an ideal adsorbent. Further, pHzpc of the prepared carbon was found to be 6.11, which suggested the surface charge of the adsorbent to be positive when $pH<pH_{zpc}$ and negative, when $pH>pH_{zpc}$ [58].

The development of porosity and enhancement of surface area is because of the reaction of KOH with biomass material. Reaction of KOH with biomass materials caused gasification and oxidation, resulting in the formation of K_2CO_3 and reduction of KOH to metallic K and H_2, as shown below by different researchers

Table 3. Physio-chemical characteristics of activated carbon at different SWB/KOH ratio

Sample ID	SWB/KOH ratio	Elemental analysis, %				Ash%	BET surface area ($m^2 g^{-1}$)	Total pore volume (cm^3g^{-1})
		C	H	N	O*			
SWAC-K06	1 : 0	64.34	2.11	0.81	28.53	4.21	112.83	0.061
SWAC-K16	1 : 1	75.98	1.90	0.66	18.00	3.46	652	0.376
SWAC-K26	1 : 2	84.25	1.29	0.70	10.92	2.84	1005.71	0.491
SWAC-K36	1 : 3	81.34	1.86	0.12	13.77	2.91	882.13	0.454

*Oxygen content %=100−(Carbon %+Nitrogen %+Hydrogen %+Ash %)

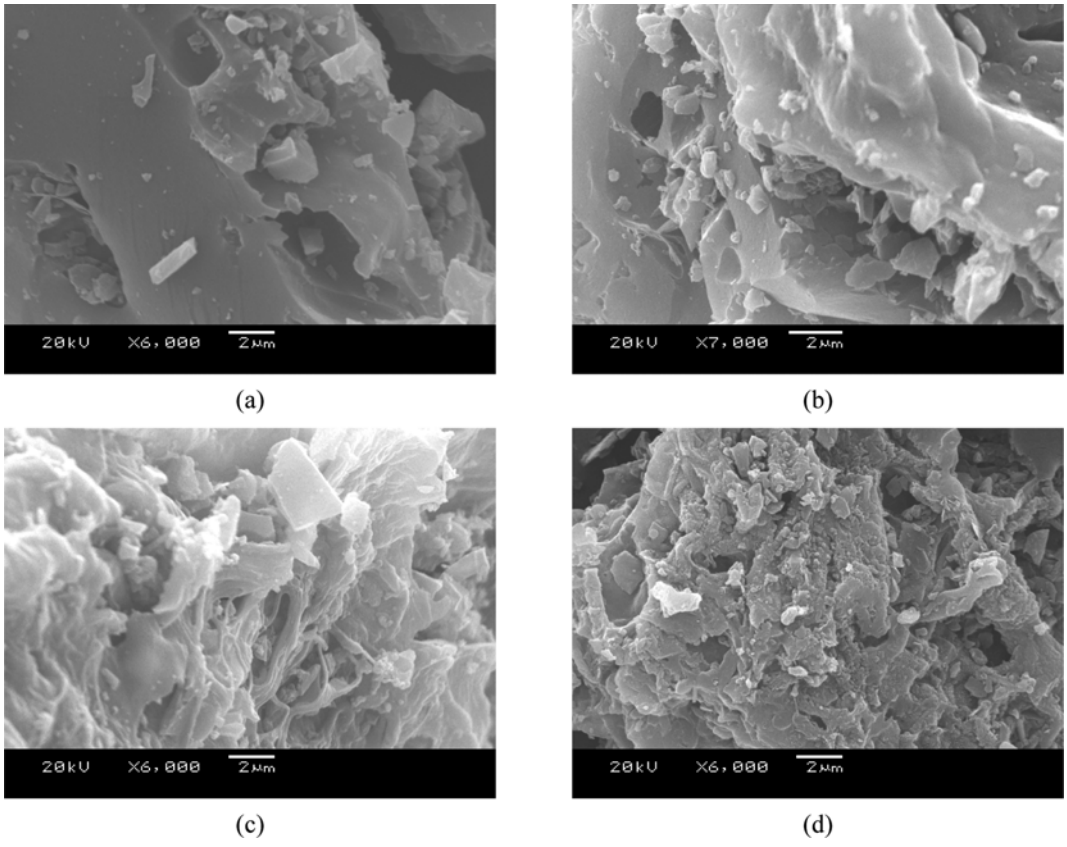

Fig. 1. SEM micrographs of (a) SWB and (b) SWAC-K16 (c) SWAC-K26 (d) SWAC-K36.

[31,33,54-56].

$$6KOH+2C\rightarrow 2K+3H_2+2K_2CO_3 \quad (1)$$

Initially, at lower temperature, KOH dehydrates to form K_2O, which reacts with in-situ formed CO_2 from the biomass to give K_2CO_3 (reactions 2 and 3). At higher temperature, K_2CO_3 further decomposes into CO and K_2O [31]. The CO_2 evolved during the decomposition process also reacts with biomass material releasing CO and the biomass material continues to react until it is completely spent and subsequently transformed into metallic K and CO at elevated temperature (reaction 4-6) [31,50,54].

$$2KOH\rightarrow K_2O+H_2O \quad (2)$$

$$K_2O+CO_2\rightarrow K_2CO_3 \quad (3)$$

$$CO_2+C\rightarrow 2CO \quad (4)$$

$$K_2CO_3+C\rightarrow K_2O+2CO \quad (5)$$

$$K_2O+C\rightarrow 2K+CO \quad (6)$$

Furthermore during activation, as the temperature is alleviated, biomass material decomposes to give off CO, CO_2 and H_2O with the part that does not decompose, resulting in the formation of char [54]. The metallic potassium reacts with the char by intercalating into the carbon matrix, subsequently leading to the development of pores during pyrolysis and the washing process. It is further possible that during the activation process, some surface metal complexes are produced that are responsible for carbon gasification, thereby releasing volatiles like CO_2, H_2 and CO [31]. Accumulation of these volatiles inside the carbon matrix creates a pressure and trapped volatiles escape out of the carbon matrix by diffusion leading to formation of pores [57]. This overall process creates a large porous structure and surface area of the carbon as reflected in Tables 2 and 3.

2. SEM Analysis of the Activated Carbon

The SEM micrographs of the carbon synthesized at 600 °C with different impregnation ratio are shown in Fig. 1(a)-(d). It can be seen in the micrograph that the surface of the carbon is without much void and generally smooth for carbon where no KOH impregnation was done (SWB, Fig. 1(a)). Whereas, for SWAC-K16 (Fig. 1(b)) impregnated with 1 : 1 ratio, minute amounts of pores are visible. But with increasing SWB/KOH ratio to 1 : 2, full of cavities with numerous cracks, pits, and pores distributed all over the surface is observed which might be due to the interaction of KOH leading to dehydrogenation and oxidation reaction during carbonization process (Fig. 1(c)). Also, thin layers within the SWAC-K26 structure along with pores could possibly be due to the release of volatiles during the carbonization process. This result corresponds to the higher BET surface area and total pore volume of 1,005.71 m^2g^{-1} and 0.491 cm^3g^{-1}, respectively. But with the addition of more amount of KOH to SWB, there was a breakdown of the carbon matrix of SWAC-K36, possibly because of the destruction of pores as shown in Fig. 1(d).

3. Crystallographic Characterization of Activated Carbon

Fig. 2 shows the X-ray diffractograms of activated carbon without impregnation and impregnated with different SWB/KOH ratio. For all the samples two broad peaks can be observed at around 2theta=~23° and ~43°, respectively, which accounts for turbostratic carbon [59]. Peaks at these ranges of scattering angle are generally associated with the (002) diffraction, which is because of the presence of stacking of graphene sheets, while a peak near 43° accounts for (101) diffraction which is due to the presence of small realms of ordered graphene sheets [27,60]. The diffractogram shows higher intensity for KOH impregnated samples as compared to samples devoid of KOH impregnation. This may be attributed to the improvement of ordering of graphitic carbon layers of the carbonaceous material by KOH activation [54].

4. Adsorption of Fluoride onto Prepared Activated Carbon

4-1. Batch Equilibrium Studies

Batch mode adsorption experiments were conducted, in which 50 ml of different initial fluoride concentration (2 mg L^{-1}, 5 mg L^{-1} and 8 mg L^{-1}) were taken in a 250 ml plastic flask on a shaker with varying adsorbent dose (0.05 g-0.3 g) at different pH (2-12) at 30 °C to investigate the optimum equilibrium condition. The adsorbent dosage was kept at 0.15 g after optimization and further experiments were performed at different contact time (2-180 mins) to set the equilibrium time. The equilibrium time was found to be 100 mins. The effect of pH on adsorption of fluoride ion was studied, keeping other parameters constant (adsorbent dose: 0.15 g,

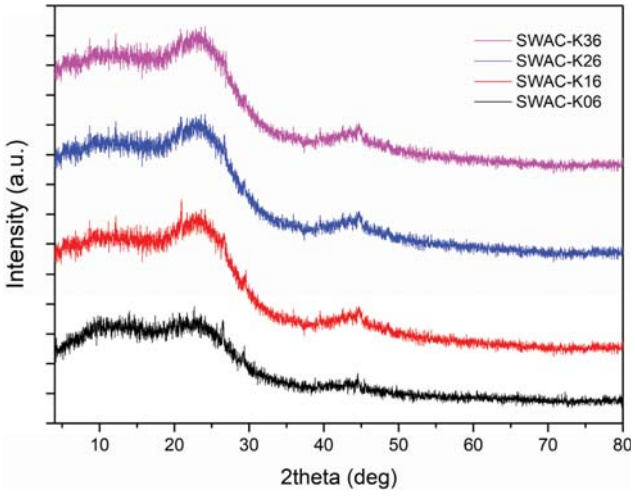

Fig. 2. XRD diffractogram of SWACs.

Table 4. Values of isotherm model for adsorption of fluoride onto SWAC

Isotherm model	Parameters	Values
Langmuir	q_{max}	2.524
	K_L	7.163
	R_L	0.027
	R^2	0.999
Freundlich	K_F	1.976
	$1/n_F$	0.298
	R^2	0.821
Temkin	A_T	153.58
	B_T	0.410
	R^2	0.975

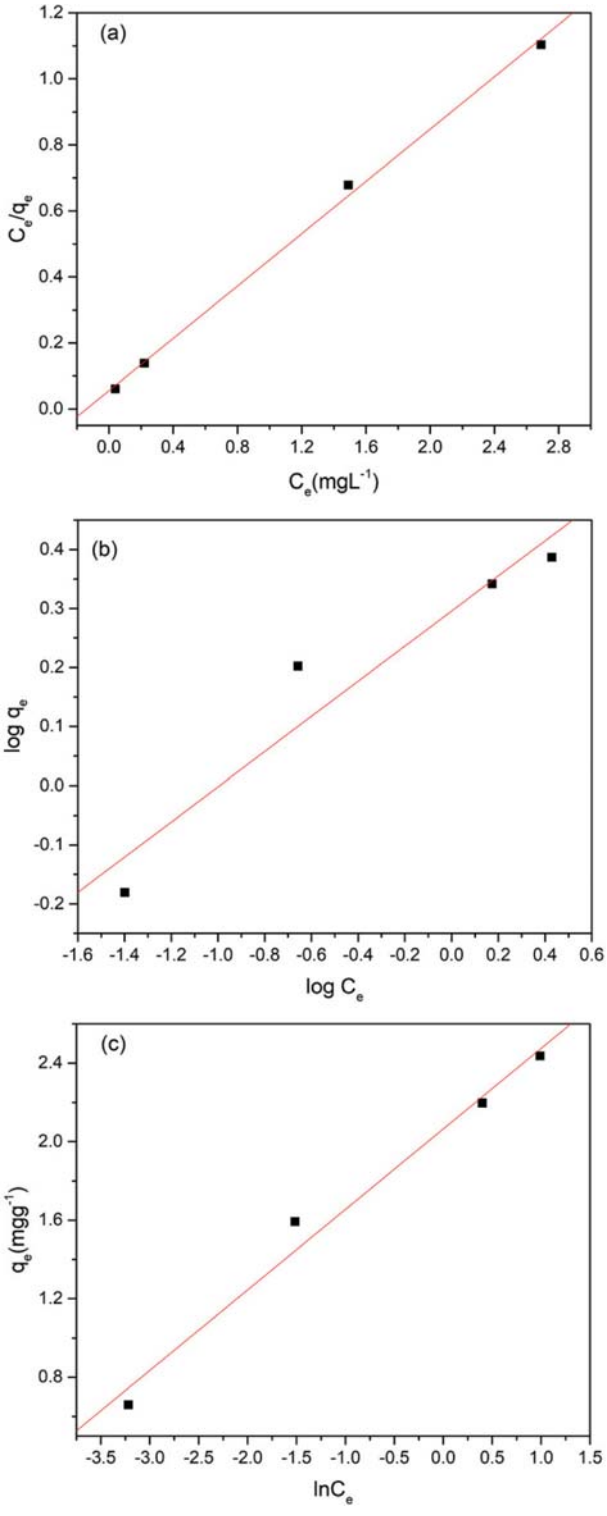

Fig. 3. Linear fitting of (a) Langmuir (b) Freundlich (c) Temkin adsorption isotherm model (Temperature=303 K, adsorbent dose=0.15 g, pH=4, contact time=100 min).

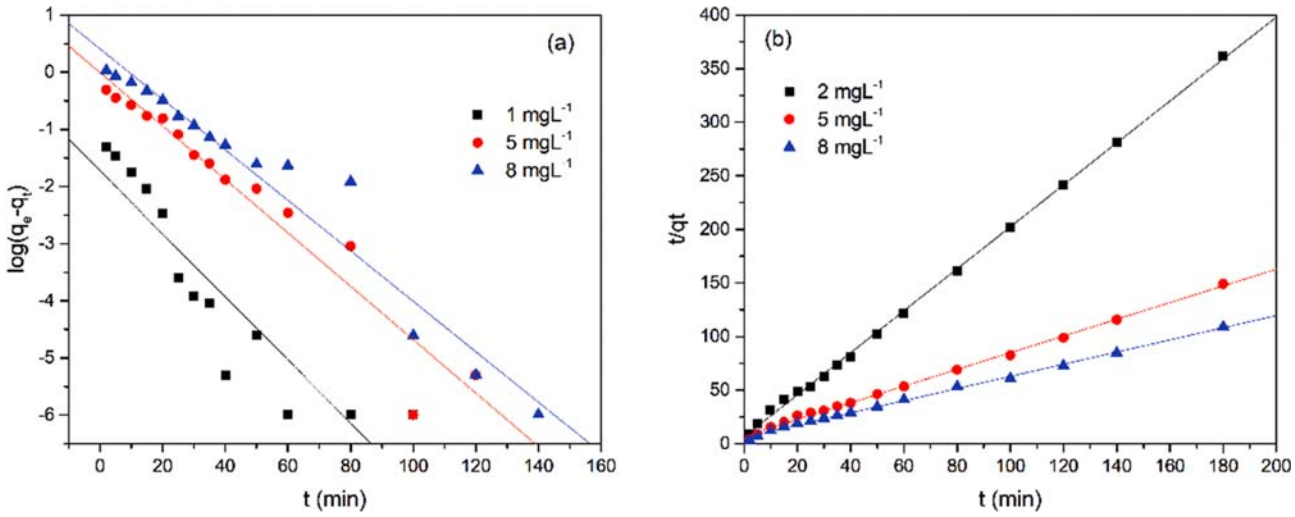

Fig. 4. Fits of (a) pseudo-first-order kinetics (b) pseudo-second-order kinetics for adsorption of fluoride.

contact time: 100 min, fluoride concentration: 50 mL of 5 mg L^{-1}). Fluoride adsorption was more pronounced at pH lower than 6, which correlates with a zero-point charge of 6.11. As the surface charge of adsorbent will be positively charged when pH is less than pH_{zpc}, therefore, at pH below 6.11, the adsorbent gains more positive charge ameliorating the adsorption of fluoride ions onto SWAC surface. All further adsorption experiments were done at a pH of 4.

4-2. Equilibrium Adsorption Isotherms

For equilibrium adsorption studies, the Langmuir and Freundlich adsorption models were analyzed with the experimental data. Langmuir isotherm is based on the assumption that adsorption is of chemical adsorption occurring on a homogeneous surface, while in Freundlich isotherm the adsorption is assumed to take place on heterogeneous surfaces [40-42]. Results obtained from the fitting of the experimental data are shown in Table 4. For the present study, q_{max} (maximum adsorption capacity) value of 2.524 mg g^{-1} with R^2 value of 0.999 was obtained for Langmuir isotherms showing a good fitting of this isotherm to the experimental data (Fig. 3(a)). The separation factor (R_L), which is an important parameter of the Langmuir isotherm, was found to be 0.027 indicating a favorable adsorption.

Further for Freundlich isotherm, the values, 1/nF<1 and 1/nF>1 specify a normal Langmuir isotherm and cooperative type of adsorption, respectively. The value obtained for 1/nF was 0.298, which indicates that the adsorption was favorable on the surface of the adsorbent. The fitting of experimental data to Freundlich isotherm gives R^2 value of 0.821 (Fig. 3(b)), which is much lower than Langmuir isotherm.

The Temkin isotherm, which considers the interaction of adsorbent-adsorbate, assumes that heat of adsorption decreases linearly with respect to surface coverage. The current experimental data when fitted to Temkin model gives the value of B_T (heat of adsorption) as 0.410, while R^2 value was found to be 0.975 (Fig. 3(c)). Thus, based on the R^2 value, the adsorption of fluoride by SWAC follows the Langmuir isotherm model, i.e., adsorption is predominantly monolayer type of adsorption.

4-3. Adsorption Kinetics

The adsorption kinetics was investigated using pseudo-first order and pseudo-second order kinetics model. Graph of $\log(q_e - q_t)$ versus t and was plotted for pseudo-first order, while graph of t/q_t versus t was plotted for pseudo-second-order kinetics model at all fluoride concentrations. Fig. 4 shows the plot of pseudo-first-order kinetics and pseudo-second order kinetics for adsorption of fluoride, and the obtained results are listed in Table 5. Table 5 shows that the measured $q_{e,meas}$ value of pseudo-first-order kinetic model was not consistent with experimental $q_{e,exp}$ values; thus, it did not fit well (Fig. 4). R^2 values for the pseudo-second-order kinetics model at all concentrations were observed to have higher value when compared with the pseudo-first-order kinetics model. Moreover, its measured equilibrium adsorption capacity, $q_{e,meas}$ was also found to be in good agreement with the values obtained by experiments, $q_{e,exp}$. Thus, it is evident that the pseudo-second order kinetics model was more suitable in describing the adsorption of fluoride onto *Schima wallichii* activated carbon. This indicates that the overall rate of fluoride adsorption is controlled predominantly by chemisorption.

Table 5. Kinetics parameter for the adsorption of fluoride onto activated carbon (SWAC)

	Pseudo-first-order kinetics				Pseudo-second-order kinetics		
C_0 (mgL^{-1})	$q_{e,exp}$ (mgg^{-1})	$q_{e,meas}$ (mgg^{-1})	k_1 (min^{-1})	R^2	$q_{e,meas}$ (mgg^{-1})	k_2 (mgg^{-1} min^{-1})	R^2
2	0.498	0.019	−0.055	0.820	0.511	0.593	0.999
5	1.215	0.983	−0.047	0.928	1.283	0.087	0.998
8	1.653	2.562	−0.044	0.947	1.761	0.053	0.997

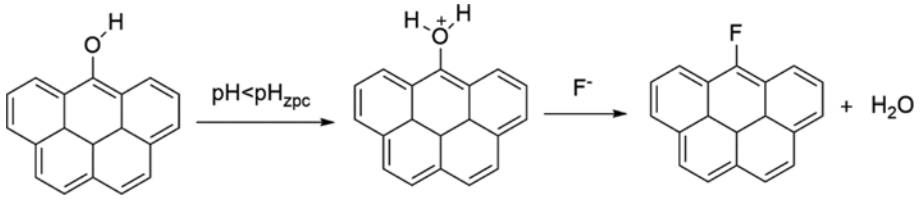

Fig. 5. A plausible mechanism of fluoride adsorption onto prepared activated carbon.

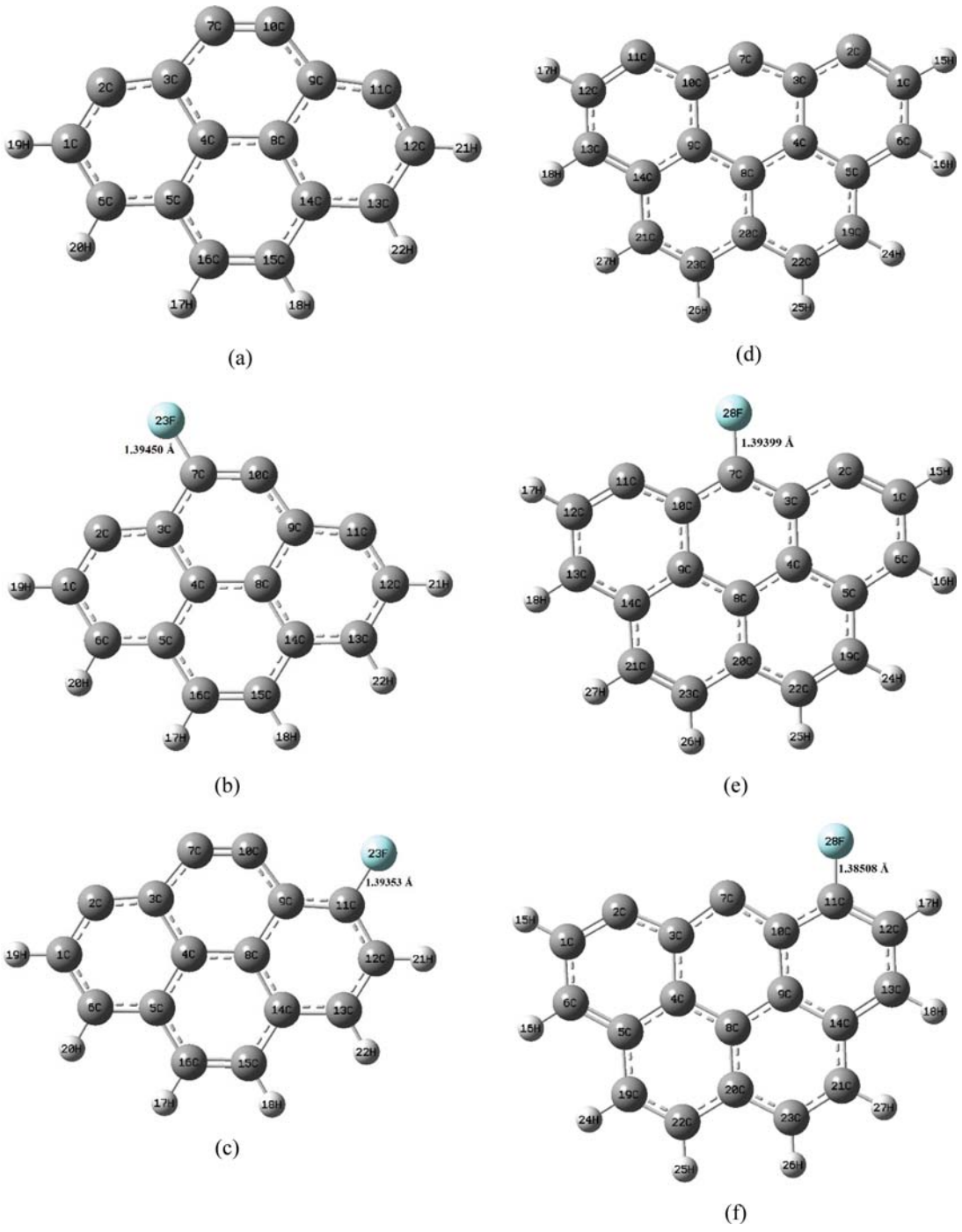

Fig. 6. Activated carbon model (a) arm-chair activated carbon (b) fluoride adsorbed onto arm-chair activated carbon (c) fluoride adsorbed onto arm-chair activated carbon edge site (d) zig-zig activated carbon model (e) fluoride adsorbed on ziz-zag activated carbon model and (f) fluoride adsorbed on zig-zag edge site.

5. Theoretical Calculations

Adsorption of fluoride generally occurs through the exchange of -OH functional groups with fluoride. Many authors have reported the mechanism on adsorption of fluoride onto adsorbent material where the -OH groups present in the adsorbent get protonated at pH less than zero point charge (acidic medium) with fluoride, which is a highly electronegative ion [58,61-64]. Also, in this current study, fluoride adsorption was found to be maximum at pH< pH_{zpc}, but when pH was increased above the zero-point charge, removal of fluoride was found to be less significant, thus confirming the exchange of -OH with fluoride to be the suitable mechanism for fluoride adsorption by deprotonation of -OH functional group present on the surface of carbon (See supplementary Fig. S1). A plausible mechanism of fluoride adsorption onto activated carbon is shown in Fig. 5.

Keeping in mind the mechanism of fluoride adsorption onto activated carbon, DFT studies were applied to understand the best possible site and orientation for the interaction of fluoride on activated carbon surface. For this study, possible models of activated carbon like arm chair model and zig-zig models, respectively, were chosen and evaluated (Fig. 6). Mulliken method was applied to generate the charge located on the atom species before and after adsorption for all possible models.

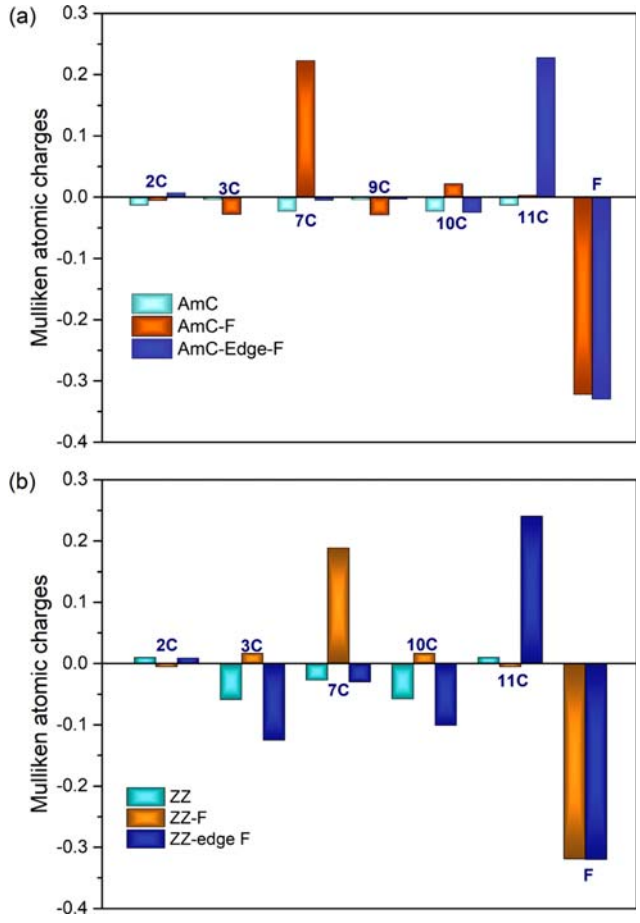

Fig. 7. Mulliken atomic charges of (a) arm chair and (b) zig-zag models.

Fig. 7 shows the Mulliken atomic charges for selected atoms of the different carbon models. Among the two adsorption sites (7C and 11C position), 11C edge site was found to be more electropositive upon adsorption of fluoride as compared to 7C site in both Arm Chair and Zig-Zag models, respectively.

This observation indicates that among the two possible adsorption sites available on the carbon models, adsorption at 11C edge site seems to be more favourable even though C-F bond formation is possible at both the sites. Further, in AmC-F (Arm chair Fluoride adsorbed at 7C position), the C-F bond length was found to be 1.39450 Å, while for AmC-Edge-F (Arm chair Fluoride adsorbed at 11C edge position) C-F bond length was 1.39353 Å which was 0.00097 Å shorter than 7C position confirming a favorable bonding of fluoride on 11C edge position.

While for ZZ-F (Zig-Zag, Fluoride adsorbed at 7C position), the bond length of C-F was found to be 1.39399 Å and for ZZ-edge-F (Zig-Zag, Fluoride adsorbed at 11C edge position), C-F bond length was 1.38508 Å which is 0.00891 Å shorter than 7C position, accounting that the adsorption of fluoride is stronger at 11C ZZ-edge-F position.

Analysis of adsorption energy of fluoride adsorbed on 7C and 11C position was found to be −69.47 kJ/mol and −193.68 kJ/mol for arm-chair model. Whereas, for Zig-Zag model adsorption energy of −139.44 kJ/mol and −143.21 kJ/mol was calculated for fluoride adsorbed on 7C and 11C position. The adsorption energy, which was found to be least at 11C edge site position in both the models, further corroborates that adsorption of fluoride takes place more favorably at 11C position rather than at 7C position.

To know the best fluoride adsorption model, the optimization of fluoride with different orientations on the activated carbon model was yielded ,and the relative energy for fluoride adsorption is illustrated in Fig. 8. From Fig. 8, fluoride has a positive affinity of adsorption onto activated carbon. However, the adsorption of fluoride on arm-chair edge site was found to be more favorable when compared with other models. The relative energy of the models and its stability follows the order: AmC-Edge-F>ZZ-Edge-F>ZZ-F>AmC-F, respectively.

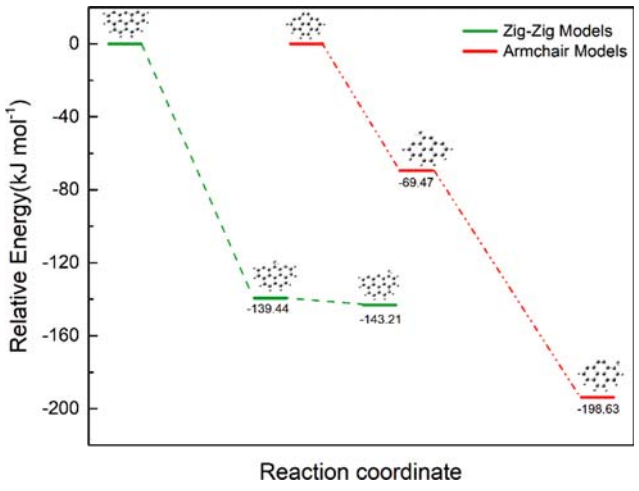

Fig. 8. Energy diagram for adsorption of fluoride onto zig-zag and arm-chair activated carbon models.

Table 6. Effect of co-ions on fluoride removal

Adsorbent	Fluoride removal in presence of co-ions (%)			
	Cl^-	NO_3^-	SO_4^{2-}	CO_3^{2-}
SWAC	90.2	87	73.4	62.2

6. Effect of Co-ions on Fluoride Adsorption

Presence of ions such as nitrate, sulfate, carbonate, chloride and bromide is usually found in fluoride-contaminated water. Their presence competes with fluoride during adsorption, decreasing the adsorption capacity of the adsorbent [3,65,66]. Adsorption of fluoride in the presence of competing anions such as chloride (Cl^-), nitrate (NO_3^-), carbonate (CO_3^{2-}) and sulphate (SO_4^{2-}) was therefore investigated by taking 20 mg l^{-1} concentration of anions and with an initial fluoride concentration of 5 mg l^{-1} by keeping pH at 7, contact time for 100 mins, temperature at 303 K and adsorbent dose of 0.15 g.

A decreasing order of effect of co-ions with respect to fluoride adsorption capacity was observed in the order $CO_3^{2-}>SO_4^{2-}>NO_3^-> Cl^-$ and the results are shown in Table 6. Among the different co-ions, the presence of sulfate and carbonates seems to have reduced the defluoridation efficiency significantly from 99% (without any co-ions) to 73.4% (in presence of sulfate) and to 62.2% (in presence of carbonate), respectively. The decrease in the removal efficiency could be because of change in the pH of the fluoride solution on addition of the competing ions. It was observed that the pH values of fluoride solution (pH=7) mixed with Cl^-, NO_3^-, SO_4^{2-} and CO_3^{2-} became 7.07, 7.18, 7.27 and 10.63, respectively. Hence, with the increase of pH, the solution mixture shifted towards the basic end, which resulted in decrease of fluoride adsorption. A similar effect of co-ions was also reported earlier by several authors [21,23,67,68].

The presence of chloride and nitrate seems to have lesser significant effect on fluoride adsorption as compared to presence of sulfate and carbonate, and this might be further due to the outer sphere surface complex formation (for chloride and nitrate). However, the presence of sulfate ions, which accounts for a lesser fluoride adsorption, could be because of outer sphere and inner sphere surface complexes [69]. On the other hand, in the presence of carbonates, the pH shifts towards the alkaline pH because of the reduction the positive charge on the active sites of the adsorbent by carbonates, and thus reduces the active sites of adsorption for fluoride, thereby lowering the removal efficiency [21,67,68].

7. Comparison of *Schima wallichii* Activated Carbon with other Adsorbents

The efficiency of fluoride adsorption onto prepared activated carbon obtained in the present work was compared with other reported adsorbents in the literature (Table 7). Maximum adsorption capacity was considered for comparison. The defluoridation capacity of *Schima wallichii* activated carbon was comparable with other adsorbents and found to be one of the good adsorbents.

CONCLUSIONS

The preparation and characterization of KOH activated carbon by single step method from *Schima wallichii* biomass was investigated and described. Optimized condition shows that activated carbon with highest porosity and BET surface area can be easily prepared by KOH activation, keeping impregnation biomass/KOH ratio of 1 : 2, temperature of 600 °C for 2 hours. BET surface area, total pore volume, carbon content and pH_{zpc} were found to be 1,005.71 m^2g^{-1}, 0.49 cm^3g^{-1}, 84.25% and 6.11, respectively, at optimized activation condition. SEM micrographs revealed that, *Schima wallichii* activated carbon have porous surface with cracks, pits and pores. XRD diffractograms show activated carbon as turbostratic carbon with ordered graphitic carbon layers. *Schima wallichii*-activated carbon shows good adsorption capacity, and adsorption of fluoride was found to be suitable under pH<6. Adsorption isotherm was found to best fit Langmuir isotherm model, which suggests a monolayer adsorption with maximum adsorption capacity of 2.524 mgg^{-1}. Kinetics study shows that adsorption was chemisorptive as it follows pseudo-second-order kinetics. Further, DFT studies also revealed favorable adsorption of fluoride on 11C edge

Table 7. Comparison of prepared activated carbon in this study with some other adsorbent reported in the literature for fluoride removal

Adsorbent	Contact time (h)	pH	Adsorbent dose (g)	Q_{max} (mg g^{-1})	References
Schima wallichii activated carbon	1.4	4	0.15	2.524	Present study
Jamun seed activated carbon	2	2.5	0.4	2.27	[58]
Diatomite	1	5	50	1.379-3.359	[3]
Activated cotton nut shells carbon	3	7	1.75	2.472	[23]
Fe_2O_3/Areca nut activated carbon composite	3	2	20	4.8	[70]
Manganese-oxide-coated alumina	-	7±0.2	5	1.10-2.85	[71]
Al and Fe dispersed in porous granular ceramics	48	6	2	1.79	[62]
Ti(IV) modified granular activated carbon	2	6-7	1	2.87	[72]
Mucuna pruriens activated carbon	3	3	1.5	0.712	[73]
Cerium impregnated activated carbon	3	6±0.2	2	4.1-4.62	[74]
Granular ferric hydroxide	2	6-7	10	3.68-5.97	[75]
Treated banana peel bioadsorbent	13	2	24	0.3950	[20]
Treated coffee husk bioadsorbent	1	2	18	0.4159	[20]
Aluminium impregnated coconut fiber	1	5	0.05	1.123	[76]

site of arm chair activated carbon model with adsorption energy of −193.68 kJ/mol, suggesting the interaction fluoride to be chemical. Thus, *Schima wallichii* biomass can serve as an effective precursor for preparation of activated carbon by KOH activation for adsorption of fluoride from aqueous water.

ACKNOWLEDGEMENTS

The authors Parimal Chandra Bhomick, Aola Supong and Rituparna Karmaker are grateful to Department of Science and Technology-INSPIRE Fellowship, Mridushmita Baruah to UGC Non-NET. The authors acknowledges SAIF-NEHU, Tezpur University for the instrumental facilities, Department of Applied Sciences, Gauhati University, for computational facility.

CONFLICT OF INTEREST

The authors declare no conflict of interest.

SUPPORTING INFORMATION

Additional information as noted in the text. This information is available via the Internet at http://www.springer.com/chemistry/journal/11814.

REFERENCES

1. WHO, Guidelines for drinking-water quality: fourth edition incorporating the frst addendum, Geneva (2017).
2. S. Jagtap, M. K. Yenkie, N. Labhsetwar and S. Rayalu, *Chem. Rev.*, **112**, 2454 (2012).
3. L. Xu, X. Gao, Z. Li and C. Gao, *Desalination*, **369**, 97 (2015).
4. P. Sehn, *Desalination*, **223**, 73 (2008).
5. A. Meenakshi and R. C. Maheshwari, *J. Hazard. Mater.*, **137**, 456 (2006).
6. M. Tahaikt, R. El Habbani, A. Ait Haddou, I. Achary, Z. Amor, M. Taky, A. Alami, A. Boughriba, M. Hafsi and A. Elmidaoui, *Desalination*, **212**, 46 (2007).
7. J. Shen and A. I. Schäfer, *Sci. Total Environ.*, **527**-**528**, 520 (2015).
8. J. Markovski, J. Garcia, K. D. Hristovski and P. Westerhoff, *Sci. Total Environ.*, **599**-**600**, 1848 (2017).
9. N. Kabay, Ö. Arar, S. Samatya, Ü. Yüksel and M. Yüksel, *J. Hazard. Mater.*, **153**, 107 (2008).
10. M. H. Dehghani, M. Farhang, M. Alimohammadi, M. Afsharnia, and G. Mckay, *Chem. Eng. Commun.*, **205**, 955 (2018).
11. Y. Zhu, H. Zhang, H. Zeng, M. Liang and R. Lu, *Int. J. Environ. Sci. Technol.*, **9**, 463 (2012).
12. J. Hayashi, A. Kazehaya, K. Muroyama and A. P. Watkinson, *Carbon N. Y.*, **38**, 1873 (2000).
13. H. Treviño-Cordero, L. G. Juárez-Aguilar, D. I. Mendoza-Castillo, V. Hernández-Montoya, A. Bonilla-Petriciolet and M. A. Montes-Morán, *Ind. Crops Prod.*, **42**, 315 (2013).
14. C. Pongener, P. Bhomick, S. Upasana Bora, R. L. Goswamee, A. Supong and D. Sinha, *Int. J. Environ. Sci. Technol.*, **14**, 1897 (2017).
15. X. J. Jin, M. Y. Zhang, Y. Wu, J. Zhang and J. Mu, *Ind. Crops Prod.*, **43**, 617 (2013).
16. I. Ozdemir, M. Şahin, R. Orhan and M. Erdem, *Fuel Process. Technol.*, **125**, 200 (2014).
17. A. Bhatnagar, E. Kumar and M. Sillanpää, *Chem. Eng. J.*, **171**, 811 (2011).
18. P. C. Bhomick, A. Supong and D. Sinha, *Int. J. Hydrol.*, **1**, 31 (2017).
19. A. Kumar and H. M. Jena, *Appl. Surf. Sci.*, **356**, 753 (2015).
20. T. Getachew, A. Hussen and V. M. Rao, *Int. J. Environ. Sci. Technol.*, **12**, 1857 (2015).
21. M. Suneetha, B. S. Sundar and K. Ravindhranath, *J. Anal. Sci. Technol.*, **6**, 15 (2015).
22. S. Kumar, A. Gupta and J. P. Yadav, *J. Environ. Biol.*, **29**, 227 (2008).
23. R. Mariappan, R. Vairamuthu and A. Ganapathy, *Chinese J. Chem. Eng.*, **23**, 710 (2015).
24. L. M. Singh, M. Kumar, B. K. Sahoo, B. K. Sapra and R. Kumar, *Phys. Procedia.*, **80**, 120 (2015).
25. C. Pongener, D. Kibami and K. S. Rao, *Chem. Sci. Trans.*, **4**, 59 (2015).
26. O. Üner, Ü. Geçgel and Y. Bayrak, *Water. Air. Soil Pollut.*, **227**, (2016).
27. D. Mohan, A. Sarswat, V. K. Singh, M. Alexandre-Franco and C. U. Pittman, *Chem. Eng. J.*, **172**, 1111 (2011).
28. C. Peng, X. Bin Yan, R. T. Wang, J. W. Lang, Y. J. Ou and Q. J. Xue, *Electrochim. Acta.*, **87**, 401 (2013).
29. L. Zhu, N. Zhao, L. Tong and Y. Lv, *RSC Adv.*, **8**, 21012 (2018).
30. P. C. Bhomick, A. Supong, M. Baruah, C. Pongener and D. Sinha, *Sustain. Chem. Pharm.*, **10**, 41 (2018).
31. J. Wang and S. Kaskel, *J. Mater. Chem.*, **22**, 23710 (2012).
32. G. Singh, I. Y. Kim, K. S. Lakhi, P. Srivastava, R. Naidu and A. Vinu, *Carbon N. Y.*, **116**, 448 (2017).
33. A.-N. A. El-Hendawy, *Appl. Surf. Sci.*, **255**, 3723 (2009).
34. X.-J. Jin, Z.-M. Yu and Y. Wu, *Cellul. Chem. Technol. Cellul. Chem. Technol.*, **46**, 79 (2012).
35. M. A. Ahmad, N. A. Ahmad Puad and O. S. Bello, *Water Resour. Ind.*, **6**, 18 (2014).
36. A. Dobashi, Y. Shu, T. Hasegawa, J. Maruyama, S. Iwasaki, Y. Shen and H. Uyama, *Electrochemistry*, **83**, 351 (2015).
37. Y. Huang, E. Ma and G. Zhao, *Ind. Crops Prod.*, **69**, 447 (2015).
38. C. Orwa, A. Mutua, R. Kindt, R. Jamnadass and S. Anthony, Agroforestree Database:a tree reference and selection guide version 4.0, 2009 (http://www.worldagroforestry.org/sites/treedbs/treedatabases.asp).
39. ASTM D 2866 –94, *Current*, **15**, 1 (1999).
40. I. Langmuir, *J. Am. Chem. Soc.*, **40**, 1361 (1918).
41. K. R. Hall, L. C. Eagleton, A. Acrivos and T. Vermeulen, *Ind. Eng. Chem. Fundam.*, **5**, 212 (1966).
42. H. M. Freundlich, *J. Phys. Chem.*, **57**, 385 (1906).
43. M. I. Temkin, *Zh. Fiz. Khim.*, **15**, 296 (1941).
44. K. S. Lagergren, *Sven. Vetenskapsakad. Handingarl.*, **24**, 1 (1898).
45. Y. S. Ho and G. McKay, *Process Biochem.*, **34**, 451 (1999).
46. M. J. Frisch, G. W. Trucks, H. B. Schlegel, G. E. Scuseria, M. A. Robb, J. R. Cheeseman, G. Scalmani, V. Barone, B. Mennucci, G. A. Petersson, H. Nakatsuji, M. Caricato, X. Li, H. P. Hratchian, A. F. Izmaylov, J. Bloino, G. Zheng, J. L. Sonnenberg, M. Hada, M. Ehara, K. Toyota, R. Fukuda, J. Hasegawa, M. Ishida, T. Nakajima, Y. Honda, O. Kitao, H. Nakai, T. Vreven, J. A. Montgomery, Jr., J. E. Peralta, F. Ogliaro, M. Bearpark, J. J. Heyd, E. Brothers, K. N. Kudin, V. N. Staroverov, T. Keith, R. Kobayashi, J. Normand, K. Raghavachari, A. Rendell, J. C.

Burant, S. S. Iyengar, J. Tomasi, M. Cossi, N. Rega, J. M. Millam, M. Klene, J. E. Knox, J. B. Cross, V. Bakken, C. Adamo, J. Jaramillo, R. Gomperts, R. E. Stratmann, O. Yazyev, A. J. Austin, R. Cammi, C. Pomelli, J. W. Ochterski, R. L. Martin, K. Morokuma, V. G. Zakrzewski, G. A. Voth, P. Salvador, J. J. Dannenberg, S. Dapprich, A. D. Daniels, O. Farkas, J. B. Foresman, J. V. Ortiz, J. Cioslowski and D. J. Fox, Gaussian 09, Revision C.01, Gaussian, Inc., Wallingford CT (2010).
47. F. Shen, J. Liu, Z. Zhang, Y. Dong and C. Gu, *Fuel Process. Technol.*, **171**, 258 (2018).
48. Y. Yang, J. Liu, B. Zhang and F. Liu, *J. Hazard. Mater.*, **321**, 154 (2017).
49. I. Okman, S. Karagöz, T. Tay and M. Erdem, *Appl. Surf. Sci.*, **293**, 138 (2014).
50. T. Tay, S. Ucar and S. Karagöz, *J. Hazard. Mater.*, **165**, 481 (2009).
51. D.-H. Jeon, S.-T. Bae and S.-J. Park, *Carbon Lett.*, **17**, 85 (2016).
52. S. Mopoung, P. Moonsri, W. Palas and S. Khumpai, *Sci. World J.*, **2015**, 1 (2015).
53. A. Nayak, B. Bhushan, V. Gupta and P. Sharma, *J. Colloid Interface Sci.*, **493**, 228 (2017).
54. G. Singh, I. Y. Kim, K. S. Lakhi, P. Srivastava, R. Naidu and A. Vinu, *Carbon*, **116**, 448 (2017).
55. D. Lozano-Castelló, J. M. Calo, D. Cazorla-Amorós and A. Linares-Solano, *Carbon N. Y.*, **45**, 2529 (2007).
56. H. Deng, G. Li, H. Yang, J. Tang and J. Tang, *Chem. Eng. J.*, **163**, 373 (2010).
57. K. Raveendran, *Fuel*, **77**, 769 (1998).
58. R. Araga, S. Soni and C. S. Sharma, *J. Environ. Chem. Eng.*, **5**, 5608 (2017).
59. G. Singh, K. S. Lakhi, I. Y. Kim, S. Kim, P. Srivastava, R. Naidu and A. Vinu, *ACS Appl. Mater. Interfaces*, **9**, 29782 (2017).
60. D. Qu, *J. Power Sources*, **109**, 403 (2002).
61. Y. Tang, X. Guan, T. Su, N. Gao and J. Wang, *Colloids Surf., A Physicochem. Eng. Asp.*, **337**, 33 (2009).
62. N. Chen, Z. Zhang, C. Feng, D. Zhu, Y. Yang and N. Sugiura, *J. Hazard. Mater.*, **186**, 863 (2011).
63. A. Bonilla-petriciolet and D. I. Mendoza-castillo, *Appl. Surf. Sci.*, **355**, 748 (2015).
64. A. A. M. Daifullah, S. M. Yakout and S. A. Elreefy, *J. Hazard. Mater.*, **147**, 633 (2007).
65. J. Zhang, N. Chen, Z. Tang, Y. Yu, Q. Hu and C. Feng, *Phys. Chem. Chem. Phys.*, **17**, 12041 (2015).
66. J. Saikia, S. Sarmah, T. H. Ahmed, P. J. Kalita and R. L. Goswamee, *J. Environ. Chem. Eng.*, **5**, 2488 (2017).
67. S. P. Kamble, S. Jagtap, N. K. Labhsetwar, D. Thakare, S. Godfrey, S. Devotta and S. S. Rayalu, *Chem. Eng. J.*, **129**, 173 (2007).
68. Y. Chen, Q. Zhang, L. Chen, H. Bai and L. Li, *J. Mater. Chem. A.*, **1**, 13101 (2013).
69. M. S. Onyango, Y. Kojima, O. Aoyi, E. C. Bernardo and H. Matsuda, *J. Colloid Interface Sci.*, **279**, 341 (2004).
70. S. Joshi and M. A. Pradhananga, *J. Inst. Eng.*, **12**, 175 (2016).
71. S. M. Maliyekkal, A. K. Sharma and L. Philip, *Water Res.*, **40**, 3497 (2006).
72. D. Tang, Y. Zhao, Y. Wang, Y. Yang, D. Li, T. Peng and X. Mao, *Desalin. Water Treat.*, **54**, 3432 (2015).
73. C. Pongener, D. Kibami, K. S. Rao and D. Sinha, *Chem. Sci. Trans.*, **4**, 59 (2015).
74. T. Raychoudhury, S. P. Boindala and S. Kalidindi, *Water Sci. Technol. Water Supply*, **17**, 1 (2017).
75. E. Kumar, A. Bhatnagar, M. Ji, W. Jung, S. Lee, S. Kim, G. Lee, H. Song, J. Choi, J. Yang and B. Jeon, *Water Res.*, **43**, 490 (2009).
76. N. K. Mondal, R. Bhaumik and J. K. Datta, *Alexandria Eng. J.*, **54**, 1273 (2015).

Supporting Information

Activated carbon synthesized from biomass material using single-step KOH activation for adsorption of fluoride: Experimental and theoretical investigation

Parimal Chandra Bhomick, Aola Supong, Rituparna Karmaker, Mridushmita Baruah, Chubaakum Pongener, and Dipak Sinha†

Department of Chemistry, Nagaland University, Lumami 798627, India
(*Received 20 October 2018 • accepted 19 January 2019*)

Functional Group Analysis of Activated Carbon

In order to understand the presence of functional group in the prepared samples, FT-IR spectra were taken and compared for prepared activated carbon along with SWB (Fig. 1S). The FT-IR spectrum of SWB was found to be comparatively parallel to many other types of biomass material [1-5]. Appearance of board peaks ~3,400 cm^{-1} are associated with O-H stretching vibration of hydrogen bonded hydroxyl functional group for both SWB and activated carbon sample [3,6]. Small peak at ~2,888 cm^{-1} could be attributed to C-H vibrational stretching from alkanes and alkyl respectively [7]. The band at 1,729 cm^{-1} accounts for C=O stretching vibrations in ketones and carboxylic acids. Bands occurring near 1,630 cm^{-1} and 1,520 cm^{-1} could be assigned for C-O vibrational stretching for quinine functional groups and C=C stretching vibration in aromatic rings [8]. Bands near 1,314 cm^{-1} could be assigned to C-O stretching vibration from ester, ether and phenolic functional groups [9]. Board bands are observed around 1,193 cm^{-1} that accounts for C-O vibrational stretching for primary and secondary alcohols. Finally, bands at 899-671 cm^{-1} may corresponds to =C-H bending for aromatic rings respectively while board peaks at ~607 cm^{-1} accounts for O-H bending [3]. A remarkable change was notice as a result of activation process. It can be seen from Fig. 1S. that most bands in the fingerprint region of *Schima wallichii* activated carbon either reduces or diminishes as compared to SWB. These disappearances of certain bands upon activation could be attributed to the dehydrogenation and oxidation reaction that takes place during activation process.

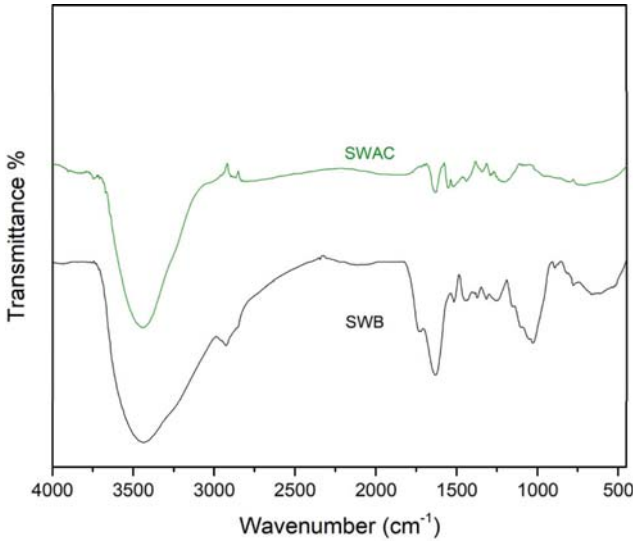

Fig. S1. FT-IR spectra of SWB and Samples impregnated at different KOH ratio carbonized at 600 °C for 2 hours.

REFERENCES

1. I. Ozdemir, M. Şahin, R. Orhan and M. Erdem, *Fuel Process. Technol.*, **125**, 200 (2014).
2. S. Mopoung, P. Moonsri, W. Palas and S. Khumpai, *Sci. World J.*, **2015**, 1 (2015).
3. A.-N. A. El-Hendawy, *Appl. Surf. Sci.*, **255**, 3723 (2009).
4. C. Pongener, D. Kibami and K. S. Rao, *Chem. Sci. Trans.*, **4**, 59 (2015).
5. A. Kumar and H. M. Jena, *Appl. Surf. Sci.*, **356**, 753 (2015).
6. D. Mohan, A. Sarswat, V. K. Singh, M. Alexandre-Franco and C. U. Pittman, *Chem. Eng. J.*, **172**, 1111 (2011).
7. M. Shariful Islam, B. Chin Ang, S. Gharehkhani and A. Binti Muhammad Afifi, *Carbon Lett.*, **20**, 1 (2016).
8. M. A. Ahmad, N. A. Ahmad Puad and O. S. Bello, *Water Resour. Ind.*, **6**, 18 (2014).
9. K. M. Doke and E. M. Khan, *Arab. J. Chem.*, **10**, S252 (2017).